

Nonlinear oscillatory convection in mushy layers

By PETER GUBA† AND M. GRAE WORSTER

Institute of Theoretical Geophysics, Department of Applied Mathematics and Theoretical Physics,
University of Cambridge, Wilberforce Road, Cambridge CB3 0WA, UK

(Received 29 April 2005 and in revised form 11 October 2005)

We study the problem of nonlinear development of oscillatory convective instability in a two-dimensional mushy layer during solidification of a binary mixture. We adopt the near-eutectic limit, making the problem analytically tractable using standard perturbation techniques. We consider also a distinguished limit of large Stefan number, which allows a destabilization of the system to an oscillatory mode of convection. We find that either travelling waves or standing waves can be supercritically stable, depending strongly on the sensitivity of permeability of the mushy layer to variations in the local solid fraction: mushy-layer systems with relatively weak sensitivity are more likely to select travelling waves rather than standing waves in the nonlinear regime. Furthermore, the decrease in permeability is found to promote the subcritical, and hence more unstable, primary oscillatory states. In addition to mapping out the location of different stable oscillatory patterns in the available parameter space, we give the detailed spatio-temporal structure of the corresponding thermal, flow and solid-fraction fields within the mushy layer, as well as the local bulk composition in the resulting eutectic solid.

1. Introduction

When a binary alloy solidifies directionally, a planar interface between the liquid and solid regions can become morphologically unstable owing to constitutional supercooling. As a consequence of this supercooling, regions of coexisting liquid and solid phases, referred to as ‘mushy’ regions, are often formed. Mushy regions are prevalent in a number of industrial and environmental contexts, including metallurgy (Flemings 1974), the Earth’s core (Fearn 1998), silicate magma chambers (Kerr & Tait 1986), sedimentary basins (Aharonov, Spiegelman, Kelemen 1997) and sea ice (Wettlaufer, Worster & Huppert 2000).

The solidification of a binary alloy in a mushy layer can be profoundly influenced by fluid flow. The flow of interstitial fluid in mushy layers can be driven by a variety of different physical mechanisms, though natural, buoyancy-driven convection has received much attention in recent years (see Worster 1997 for a review). In binary alloys cooled from below, compositional convection can be driven by unstable density gradients generated as the denser constituent of the alloy is preferentially incorporated within the solid, making the residual liquid within the mushy layer compositionally buoyant.

Linear stability analyses allow one to find the critical conditions at which convective instabilities of infinitesimal amplitudes first occur. Nevertheless, it was anticipated

† Present address: Department of Applied Mathematics and Statistics, Faculty of Mathematics, Physics and Informatics, Comenius University, 842 48 Bratislava, Slovakia.

(Fowler 1985; Worster 1992) that the steady convective instability in the mushy layer would be subcritically unstable. This issue has been confirmed by weakly nonlinear analyses of Amberg & Homsy (1993) and Anderson & Worster (1995) who investigated a relatively simple model in which the mushy layer is dynamically isolated from the liquid region above and the solid region below, and the position of the mush–liquid interface was taken to be fixed.

Chen, Lu & Yang (1994) performed a linear stability analysis of convection in a mushy layer and identified the possibility of oscillatory onset. Based on a model in which the mushy layer is coupled with the overlying liquid layer, their analysis suggests that the oscillations arise from the linear interaction between the double-diffusive convection in the liquid region and convection in the mushy layer. However, as a result of an intricate interaction between solidification and heat transfer, convective motion within the mushy layer can be oscillatory at onset even when the level of stabilizing thermal buoyancy is set equal to zero and no double-diffusive effects are present in the system (Anderson & Worster 1995). In particular, it was recognized (Anderson & Worster 1996) that the physical mechanism behind this new type of oscillatory instability is linked to a phase lag between the background macroscopic solidification as heat is withdrawn at a uniform rate from the bottom of the system, and the local dissolution caused by the fluid motion. In the spirit of Schluter, Lortz & Busse (1965), Riahi (2002) has analysed the nonlinear stability properties of these oscillatory convecting states. He considered a limit in which the permeability of the mushy layer was insensitive to the dominant linear variations in the local solid fraction. As a result, the bifurcation to oscillatory solutions was found to be always supercritical. Riahi's (2002) calculations seemed to show that, in the rather restricted parameter regime considered, no three-dimensional periodic pattern could be stable, and that either two-dimensional travelling or standing waves could be stable.

In this paper, we study the nonlinear development of the oscillatory convective instability identified by Anderson & Worster (1995) further. We consider a limit in which the leading-order behaviour of the mushy layer corresponds to that of a non-reacting porous medium with uniform permeability. Unlike Anderson & Worster (1995) and Riahi (2002), however, we impose no further constraint on the form of constitutive relationship between the permeability and the local solid fraction, thus capturing a much wider range of possible morphologies exhibited by the solid phase of the mushy layer. We perform a weakly nonlinear stability analysis to resolve which of travelling or standing waves will occur near onset of compositional convection, treating the travelling and standing waves in a unified way. A key finding of our analysis is a set of coupled nonlinear evolution equations that describes the competition of two counter-propagating waves arising via a primary Hopf bifurcation. Our results yield necessary conditions for the stability of, and the relative stability between, the travelling and standing waves in the two-dimensional mushy-layer systems, and form a basis for establishing the complete description of the possible nonlinear interactions between both types of wave-like convective motion and steady convection. Mapping out the whole parameter space available for the oscillatory instability, we provide the first systematic study of the development of nonlinear oscillatory convection in mushy layers, of which the previous nonlinear analyses represent special limiting cases.

The plan of the paper is as follows. In §2 we formulate our problem mathematically, and take a particular asymptotic limit of the governing equations which both allows the presence of an oscillatory convective instability and makes the problem analytically tractable. In §3 we perform a weakly nonlinear stability analysis and derive the

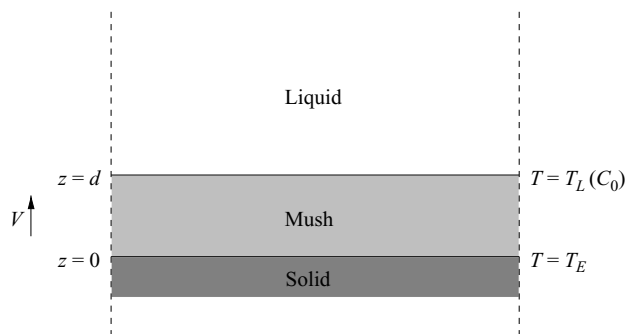


FIGURE 1. A schematic diagram of the system under consideration, showing the solid, mush, and liquid. The system is continuously being solidified at speed V in the vertical direction. The mushy layer is assumed to have constant thickness d . The bottom boundary $z=0$ of the mushy layer is kept at the eutectic temperature T_E , and the top boundary $z=d$ at the liquidus temperature $T_L(C_0)$. The top and bottom boundaries of the mushy layer are taken to be rigid, impermeable and isothermal. Mixture with concentration C_0 is fed into the mushy layer through the mush–liquid interface.

amplitude equations which govern the evolution of the finite-amplitude oscillatory convecting states. In §4 we interpret the results in terms of the stability and structure of the nonlinear oscillatory patterns. Finally, we give the conclusions in §5.

2. Formulation

The physical system under consideration consists of a horizontal mushy layer lying between a completely solid region and a completely liquid region, as illustrated in figure 1. The system is cooled uniformly from below such that the solid–mush and mush–liquid interfaces advance upwards with a constant solidification velocity V . We adopt a simplification that the mushy layer is dynamically isolated from the rest of the system (Amberg & Homsy 1993) by assuming the top and bottom boundaries of the mushy layer to be non-deformable, impermeable to fluid flow and isothermal. The system will be studied in a frame of reference moving upwards with velocity V relative to the solid formed at the bottom of the mushy layer and the solid dendrites within the mushy layer, allowing the non-convecting basic state to be independent of time. In this frame of reference, the bottom boundary of the mushy layer $z=0$ is kept at the eutectic temperature $T = T_E$, while the top boundary $z=d$ is kept at the liquidus temperature $T_L(C_0)$ and is a surface through which mixture of composition C_0 is supplied.

The temperature T and composition C of the liquid in the mushy layer are required to satisfy a linear liquidus relationship

$$T = T_L(C) \equiv T_L(C_0) + \Gamma(C - C_0), \quad (2.1)$$

where Γ is a constant. The liquid is assumed to be Newtonian with a linearized equation of state

$$\rho_l = \rho_0[1 + \beta(C - C_0)], \quad (2.2)$$

where ρ_0 is a reference density, $\beta = \beta^* - \alpha^*\Gamma$, and α^* and β^* are the constant expansion coefficients for heat and solute, respectively. The compositional effect usually dominates the thermal effect so that β is typically positive and leads to convection driven primarily by compositional buoyancy.

We start with a non-dimensional form of the governing equations which is most similar to that of Worster (1992). In this formulation all material properties are assumed to be constant and independent of phase. The fluid velocity is scaled with the prescribed solidification velocity V , length and time with the thermal-diffusion lengthscale and timescale, κ/V and κ/V^2 , and pressure with $\kappa\mu/\Pi(0)$. Here, κ is the thermal diffusivity, μ is the dynamic viscosity of the liquid and $\Pi(0)$ is the reference value of permeability of the mushy layer. The dimensionless variable for both the temperature and composition is defined by

$$\theta = [T - T_L(C_0)]/\Delta T = (C - C_0)/\Delta C, \quad (2.3)$$

where $\Delta T = \Gamma\Delta C = T_L(C_0) - T_E$, $\Delta C = C_0 - C_E$ and C_E is the eutectic composition.

The dimensionless equations representing conservation of heat, solute, momentum and mass in the reference frame translating with the eutectic front then assume the forms

$$\left(\frac{\partial}{\partial t} - \frac{\partial}{\partial z}\right)(\theta - S\phi) + \mathbf{u} \cdot \nabla\theta = \nabla^2\theta, \quad (2.4a)$$

$$\left(\frac{\partial}{\partial t} - \frac{\partial}{\partial z}\right)[(1 - \phi)\theta + \mathcal{C}\phi] + \mathbf{u} \cdot \nabla\theta = 0, \quad (2.4b)$$

$$K(\phi)\mathbf{u} = -\nabla p - Ra\theta\hat{z}, \quad (2.4c)$$

$$\nabla \cdot \mathbf{u} = 0. \quad (2.4d)$$

The dependent variables in these equations are the temperature θ , the local solid fraction ϕ , the Darcy fluid velocity \mathbf{u} and the hydrodynamic pressure p . The function $K(\phi)$ defined by $K(\phi) = \Pi(0)/\Pi(\phi)$ accounts for the variations of permeability Π with the local solid fraction ϕ . We follow Worster (1992) in assuming a constitutive expression for $\Pi(\phi)$ in which the permeability remains finite as the solid fraction approaches zero (see equation (2.15) below).

The dimensionless parameters introduced in the governing equations (2.4) are the Stefan number, the concentration ratio and the Rayleigh number,

$$S = \frac{L}{c_l\Delta T}, \quad \mathcal{C} = \frac{C_S - C_0}{C_0 - C_E}, \quad Ra = \frac{\beta\Delta Cg\Pi(0)}{\nu V}, \quad (2.5a-c)$$

respectively, where L is the latent heat of solidification, c_l is the specific heat, C_S is the composition of the solid phase forming the dendrites and g is the acceleration due to gravity. The Stefan number S expresses the ratio of the latent heat to the sensible heat. The concentration ratio \mathcal{C} represents the compositional contrast between solid and liquid phases compared to the characteristic variation of composition across the mushy layer. Note that \mathcal{C} is large when the initial composition C_0 is close to the eutectic composition C_E , as we shall consider later. The Rayleigh number Ra relates the destabilizing effect of compositional buoyancy to the stabilizing influence of viscous dissipation in the porous medium.

Equations (2.4) are augmented by boundary conditions (Amberg & Homsy 1993) that reflect the simplifying steps taken to study the dynamics of the mushy layer free from coupling with the liquid region. These boundary conditions are

$$\theta = -1, \quad w = 0 \quad \text{on} \quad z = 0, \quad (2.6a, b)$$

$$\theta = 0, \quad w = 0, \quad \phi = 0 \quad \text{on} \quad z = \delta, \quad (2.7a-c)$$

where $\delta = d/(\kappa/V)$ is the dimensionless thickness of the mushy layer and w is the z -component of \mathbf{u} . The temperature is fixed and the vertical velocity is zero on both

boundaries. In addition, the solid fraction is set to zero at the top of the mush. For a more detailed discussion of these boundary conditions the reader is referred to Anderson & Worster (1995). In place of the no-through-flow condition (2.7*b*), Chung & Chen (2000) considered a more realistic, but mathematically less convenient, constant-pressure condition in their nonlinear analysis of steady convection. Their results showed that an oscillatory instability was still possible, though at slightly modified parameter values (see also §6 of Anderson & Worster 1996), indicating that a mechanism controlling the presence of oscillations is not compromised by the imposition of the idealized condition (2.7*b*).

We proceed by reducing the model asymptotically. First, following Amberg & Homsy (1993), we study a limit in which the thickness of the mushy layer is much less than the diffusion lengthscale, by letting $\delta \ll 1$. Secondly, we assume that the compositional ratio is large by writing

$$\mathcal{C} = \bar{\mathcal{C}}/\delta, \quad \text{with } \bar{\mathcal{C}} = O(1) \quad \text{as } \delta \rightarrow 0, \tag{2.8}$$

which corresponds to the near-eutectic approximation introduced by Fowler (1985). Thirdly, we consider the limit in which the Stefan number is large (Emms & Fowler 1994) by taking

$$S = \bar{S}/\delta, \quad \text{with } \bar{S} = O(1) \quad \text{as } \delta \rightarrow 0, \tag{2.9}$$

which corresponds to the situation in which the latent heat liberated during the local phase change is much larger than the heat associated with the typical variations of temperature within the mushy layer. Note that it is this particular scaling which allows the destabilization of the mushy-layer system to the oscillatory mode of convection to be captured (Anderson & Worster 1995).

Analysis of the balances in equations (2.4) for these asymptotic limits then indicates the following rescaling of the problem:

$$(x, z) = \delta(\bar{x}, \bar{z}), \quad t = \delta^2 \bar{t}, \quad R^2 = \delta Ra, \tag{2.10a-c}$$

$$\theta = \theta_B(\bar{z}) + \epsilon \hat{\theta}(\bar{x}, \bar{z}, \bar{t}), \tag{2.10d}$$

$$\phi = \phi_B(\bar{z}) + \epsilon \hat{\phi}(\bar{x}, \bar{z}, \bar{t}), \tag{2.10e}$$

$$\mathbf{u} = \mathbf{0} + \epsilon \frac{R}{\delta} \hat{\mathbf{u}}(\bar{x}, \bar{z}, \bar{t}), \tag{2.10f}$$

$$p = Rp_B(\bar{z}) + \epsilon R \hat{p}(\bar{x}, \bar{z}, \bar{t}), \tag{2.10g}$$

where subscript *B* denotes a non-convecting basic state, in the moving frame, which is perturbed by the small convective disturbances measured by a perturbation parameter ϵ . Note that the basic state is steady and horizontally uniform, while the two-dimensional disturbances can vary in the vertical and horizontal directions, and in time.

The approximate basic-state solutions to the problem, consisting of equations (2.4), (2.6) and (2.7), under the particular asymptotic limits given by (2.8) and (2.9), can be obtained as series expansions in powers of δ , yielding

$$\theta_B = -(1 - \bar{z}) + \delta \frac{\Omega}{2} \bar{z}(1 - \bar{z}) + O(\delta^2), \tag{2.11a}$$

$$\phi_B \equiv \delta \bar{\phi}_B = \delta \frac{1}{\bar{\mathcal{C}}} (1 - \bar{z}) - \delta^2 \left(\frac{1}{\bar{\mathcal{C}}^2} (1 - \bar{z})^2 + \frac{\Omega}{2\bar{\mathcal{C}}} \bar{z}(1 - \bar{z}) \right) + O(\delta^3), \tag{2.11b}$$

where the $O(1)$ parameter $\Omega = 1 + \bar{S}/\bar{\mathcal{C}}$ represents a measure of the coupling between the thermal and solid-fraction fields. Note that ϕ_B is vanishing and θ_B is linear in

the limit $\delta \rightarrow 0$, the results directly related to the problem of convection onset in a non-reacting porous layer as studied by Palm, Weber & Kvernfold (1972). It is the higher-order terms in δ that are associated with effects pertinent to the mushy-layer system.

The equations governing convective, in general nonlinear, perturbations are

$$\left(\frac{\partial}{\partial \bar{t}} - \delta \frac{\partial}{\partial \bar{z}}\right) \left(\hat{\theta} - \frac{\bar{S}}{\delta} \hat{\phi}\right) + R \hat{w} \frac{d\theta_B}{d\bar{z}} - \nabla^2 \hat{\theta} = -\epsilon R \hat{\mathbf{u}} \cdot \nabla \hat{\theta}, \quad (2.12a)$$

$$\left(\frac{\partial}{\partial \bar{t}} - \delta \frac{\partial}{\partial \bar{z}}\right) \left((1 - \delta \bar{\phi}_B) \hat{\theta} - \theta_B \hat{\phi} - \epsilon \hat{\theta} \hat{\phi} + \frac{\bar{C}}{\delta} \hat{\phi}\right) + R \hat{w} \frac{d\theta_B}{d\bar{z}} = -\epsilon R \hat{\mathbf{u}} \cdot \nabla \hat{\theta}, \quad (2.12b)$$

$$\nabla^2 [K(\delta \hat{\phi}_B + \epsilon \hat{\phi}) \hat{u}] - \frac{\partial}{\partial \bar{x}} [\hat{\mathbf{u}} \cdot \nabla K(\delta \hat{\phi}_B + \epsilon \hat{\phi})] - R \frac{\partial^2 \hat{\theta}}{\partial \bar{x} \partial \bar{z}} = 0, \quad (2.12c)$$

$$\nabla^2 [K(\delta \hat{\phi}_B + \epsilon \hat{\phi}) \hat{w}] - \frac{\partial}{\partial \bar{z}} [\hat{\mathbf{u}} \cdot \nabla K(\delta \hat{\phi}_B + \epsilon \hat{\phi})] + R \frac{\partial^2 \hat{\theta}}{\partial \bar{x}^2} = 0, \quad (2.12d)$$

with the boundary conditions

$$\hat{\theta} = 0, \quad \hat{w} = 0 \quad \text{on} \quad \bar{z} = 0, \quad (2.13a, b)$$

$$\hat{\theta} = 0, \quad \hat{w} = 0, \quad \hat{\phi} = 0 \quad \text{on} \quad \bar{z} = 1. \quad (2.14a-c)$$

An important feature of the dynamics of the mushy layer is the variation of the permeability with the local solid fraction. Here, since the basic-state solid fraction is small, of $O(\delta)$, and the perturbation to the solid fraction is also expected to be small in the context of the weakly nonlinear theory to be developed, we expand the function $K(\phi)$ in a regular series for $\phi \ll 1$

$$K(\phi) = 1 + K_1 \phi + K_2 \phi^2 + O(\phi^3), \quad (2.15)$$

where K_1 and K_2 are constants specifying a particular form of the constitutive relationship. Note that K_1 has to be positive in order to ensure the decreasing of the permeability $\Pi(\phi)$ with increasing solid fraction ϕ . In contrast to Anderson & Worster (1995) and Riahi (2002) who kept $K_1 = O(\delta)$, no such restriction on K_1 is made in the present analysis, i.e. K_1 is formally assumed to be $O(1)$ in the limit $\delta \rightarrow 0$. The results derived with K_1 treated in this way can readily be reduced to the particular case of small K_1 studied by Anderson & Worster (1995) and Riahi (2002), and we shall recover results for that case.

3. Weakly nonlinear stability theory

Following a standard weakly nonlinear approach (e.g. Malkus & Veronis 1958; Veronis 1959), our main aim is to derive some fundamental results which are basic to the understanding of the behaviour of oscillatory convective perturbations when nonlinear interactions become important.

We seek nonlinear oscillatory solutions of (2.12)–(2.14) with frequency ω . In order to pursue a nonlinear analysis with both $\epsilon \ll 1$ and $\delta \ll 1$, it is necessary to consider the double expansions in ϵ and δ for the perturbation quantities, which we assume in the forms

$$\hat{\theta} = (\theta_{00} + \delta \theta_{01} + \dots) + \epsilon (\theta_{10} + \delta \theta_{11} + \dots) + \epsilon^2 (\theta_{20} + \delta \theta_{21} + \dots) + \dots, \quad (3.1a)$$

$$\begin{aligned} \Omega \hat{\phi} &= (\phi_{00} + \delta \phi_{01} + \dots) + \epsilon (\phi_{10} + \delta \phi_{11} + \dots) \\ &+ \epsilon^2 (\delta^{-1} \phi_{2(-1)} + \phi_{20} + \delta \phi_{21} + \dots) + \dots, \end{aligned} \quad (3.1b)$$

$$\Omega^{1/2}\hat{\mathbf{u}} = (\mathbf{u}_{00} + \delta\mathbf{u}_{01} + \dots) + \epsilon(\mathbf{u}_{10} + \delta\mathbf{u}_{11} + \dots) + \epsilon^2(\mathbf{u}_{20} + \delta\mathbf{u}_{21} + \dots) + \dots, \quad (3.1c)$$

$$\Omega^{1/2}\mathbf{R} = (\mathbf{R}_{00} + \delta\mathbf{R}_{01} + \dots) + \epsilon(\mathbf{R}_{10} + \delta\mathbf{R}_{11} + \dots) + \epsilon^2(\mathbf{R}_{20} + \delta\mathbf{R}_{21} + \dots) + \dots, \quad (3.1d)$$

$$\omega = (\omega_{00} + \delta\omega_{01} + \dots) + \epsilon(\omega_{10} + \delta\omega_{11} + \dots) + \epsilon^2(\omega_{20} + \delta\omega_{21} + \dots) + \dots. \quad (3.1e)$$

As the problem involves two small parameters, ϵ and δ , care is required with regard to their relative sizes. Here, we assume that $0 \leq \epsilon \ll \delta \ll 1$, since we expect finite-amplitude results to hold as long as $\epsilon \ll 1$. Note the appearance of a singular term in the expansion for $\hat{\phi}$ at $O(\epsilon^2)$ as $\delta \rightarrow 0$. Thus, in order for the asymptotic representation of $\hat{\phi}$ to be well defined, we further assume that $\epsilon^2 \ll \delta$. As described in the analysis of Anderson & Worster (1995), who studied the nonlinear evolution of steady patterns, the inclusion of this term is necessary in order to balance a driving term of $O(\epsilon^2\delta^{-1})$ in the solute balance (2.12*b*). In the present, oscillatory context, we shall see that the correct treatment of this term has important ramifications in terms of the stability of nonlinear oscillatory states.

We explicitly exhibit the unknown frequency ω (Veronis 1959) and introduce a slow timescale $\tau = \epsilon^2\bar{t}$ in (2.12*a, b*) by means of a transformation $\partial/\partial\bar{t} \mapsto \omega\partial/\partial\bar{t} + \epsilon^2\partial/\partial\tau$. Expressions (3.1) are then substituted into a rescaled version of (2.12)–(2.14), equation sets are generated by grouping terms of different powers of $\epsilon^m\delta^n$ ($m = 0, 1, 2, \dots; n = -1, 0, 1, \dots$), and the solutions of known period, 2π , are sought. The procedure rapidly becomes algebraically cumbersome and hence, for brevity, we shall confine ourselves to an outline of the principal results.

At $O(\epsilon^0\delta^{-1})$, we find from (2.12*a*) and (2.12*b*) that

$$\bar{S}\omega_{00} \frac{\partial\phi_{00}}{\partial\bar{t}} = 0, \quad \bar{C}\omega_{00} \frac{\partial\phi_{00}}{\partial\bar{t}} = 0. \quad (3.2a, b)$$

These equations are solved by taking $\omega_{00} = 0$. As pointed out by Anderson & Worster (1996), this result implies that a timescale of the oscillations is $O(\delta)$, rather than the $O(\delta^2)$ suggested by the initial rescaling (2.10*b*).

At the next order, $O(\epsilon^0\delta^0)$, we recover the equations defining the linear stability problem studied by Anderson & Worster (1996). In terms of the time \bar{t} , the general solutions at this order take the form

$$\theta_{00} = -\sin(\pi\bar{z})\eta_{00}(\bar{x}, \bar{t}, \tau) + \text{c.c.}, \quad (3.3a)$$

$$\phi_{00} = -\frac{1}{\bar{C}} \frac{\pi(\pi^2 + k^2)}{\pi^2 - \omega_{01}^2} \left[e^{i\omega_{01}(\bar{z}-1)} + \cos(\pi\bar{z}) + \frac{i\omega_{01}}{\pi} \sin(\pi\bar{z}) \right] \eta_{00}(\bar{x}, \bar{t}, \tau) + \text{c.c.}, \quad (3.3b)$$

$$u_{00} = \frac{\pi}{k} \cos(\pi\bar{z}) \frac{\partial\eta_{00}(\bar{x}, \bar{t}, \tau)}{\partial\bar{x}} + \text{c.c.}, \quad (3.3c)$$

$$w_{00} = k \sin(\pi\bar{z})\eta_{00}(\bar{x}, \bar{t}, \tau) + \text{c.c.}, \quad (3.3d)$$

$$R_{00} = \frac{\pi^2 + k^2}{k}, \quad (3.3e)$$

where the one-dimensional planform function is given by

$$\eta_{00}(\bar{x}, \bar{t}, \tau) = A_{00}(\tau)e^{ik\bar{x}}e^{i\omega\bar{t}} + B_{00}(\tau)e^{-ik\bar{x}}e^{i\omega\bar{t}}. \quad (3.4)$$

Here, A_{00} and B_{00} are the leading-order complex amplitudes of leftward and rightward travelling waves, respectively, and k is the horizontal wavenumber of the perturbation. A standing wave pattern is represented by $A_{00} = B_{00}$.

At the Hopf bifurcation, the frequency of the oscillatory convection is ω_{01} . In order to determine ω_{01} , involved in the leading-order solutions (3.3), it is necessary to pursue the perturbation analysis further. Specifically, at $O(\epsilon^0\delta^1)$, we find an

inhomogeneous system of equations which admits a solution only if its homogeneous part is orthogonal to all solutions of the adjoint homogeneous problem. We find that the real part of this solvability condition determines the linear Rayleigh number correction R_{01} as a function of k and ω_{01} ,

$$\frac{R_{01}}{R_{00}} = \frac{1}{4} \frac{K_1}{\bar{\mathcal{C}}} + \left[\frac{1}{4} + \frac{\pi^2(1 + \cos \omega_{01})}{(\pi^2 - \omega_{01}^2)^2} \right] \frac{\bar{S}}{\Omega^2 \bar{\mathcal{C}}^2}, \tag{3.5a}$$

and the imaginary part determines ω_{01} as a function of k ,

$$0 = \omega_{01} \left[1 + \frac{\pi^2 + k^2}{\pi^2 - \omega_{01}^2} \left(1 - \frac{2\pi^2}{\pi^2 - \omega_{01}^2} \frac{\sin \omega_{01}}{\omega_{01}} \right) \frac{\bar{S}}{\Omega^2 \bar{\mathcal{C}}^2} \right]. \tag{3.5b}$$

A careful account of the linear stability properties of the neutral oscillatory mode determined from (3.5a, b), as well as of the transition between the real convective mode and the oscillatory mode in terms of the stability boundaries in the parameter space can be found in Anderson & Worster (1996).

The $O(\epsilon^0 \delta^1)$ correction terms in expressions (3.1a–c) take rather complicated forms and are therefore not recorded here, except to note that they comprise the particular responses forced by the leading-order solutions (3.3), and the solutions to the homogeneous problem analogous to (3.3) with $\eta_{00}(\bar{x}, \bar{t}, \tau)$ replaced by

$$\eta_{01}(\bar{x}, \bar{t}, \tau) = A_{01}(\tau) e^{ik\bar{x}} e^{i\omega\bar{t}} + B_{01}(\tau) e^{-ik\bar{x}} e^{i\omega\bar{t}}. \tag{3.6}$$

By linearly combining solutions found at $O(\epsilon^0 \delta^0)$ and $O(\epsilon^0 \delta^1)$, we find that the amplitudes of interest can be defined as $\mathcal{A} \equiv A_{00} + \delta A_{01}$ and $\mathcal{B} \equiv B_{00} + \delta B_{01}$. In what follows, we shall determine how the nonlinear terms affect the evolution of \mathcal{A} and \mathcal{B} at large times, \bar{t} .

At $O(\epsilon^1 \delta^{-1})$, the relevant set of equations is given by (3.2) except that ω_{00} is now replaced by ω_{10} . These equations are solved by setting $\omega_{10} = 0$.

The solvability of the $O(\epsilon^1 \delta^0)$ and $O(\epsilon^1 \delta^1)$ systems of equations requires

$$R_{10} = 0 \quad \text{and} \quad R_{11} = 0, \quad \omega_{11} = 0, \tag{3.7a–c}$$

respectively. These results can be traced to the symmetry of the nonlinear terms in the perturbation equations (2.12). In view of the results that $\omega_{10} = 0$ and $\omega_{11} = 0$, it follows that it is not until at least $O(\epsilon^2 \delta^0)$ that the nonlinear detuning, ω_{20} , of the Hopf-bifurcation frequency, ω_{01} , is determined. (Note: We believe that Riahi (2002, §3) incorrectly states that ω_{20} is fixed at zero by virtue of the solvability condition at $O(\epsilon^2 \delta^{-1})$. Instead, at $O(\epsilon^2 \delta^{-1})$ we shall find a system (see equation (3.8) below) which is integrable without any adjustment of free quantities appearing in (3.1).)

Further vital reinforcement of the linear oscillatory convection mode takes place at $O(\epsilon^2 \delta^{-1})$. In particular, from the solute balance (2.12b), we obtain

$$\bar{\mathcal{C}} \left(\omega_{01} \frac{\partial}{\partial \bar{t}} - \frac{\partial}{\partial \bar{z}} \right) \phi_{2(-1)} = -\bar{\mathcal{C}} \left(\omega_{20} \frac{\partial}{\partial \bar{t}} + \frac{\partial}{\partial \tau} \right) \phi_{00}, \tag{3.8}$$

where ω_{20} is, as yet, undetermined. A similar balance is provided by the heat conservation (2.12a); cf. (3.2a) and (3.2b). The balance expressed by (3.8) reflects that there are two natural timescales associated with the nonlinear development of the oscillatory mode. The faster timescale, of $O(\epsilon^2)$, is that associated with the growth rate of perturbations, while the slower timescale, of $O(\delta)$, is that associated with the period of the oscillatory convection itself. In passing, we remark that there is also a third, intermediate timescale, of $O(\delta^2)$, that is characteristic of thermal diffusion;

however, this process plays only a passive role in that it is not fundamental in sustaining oscillatory motions in the system.

Finally, we arrive at the stage at which the desired evolution of the nonlinear oscillatory disturbances can be determined. Specifically, by combining the solvability conditions at $O(\epsilon^2\delta^0)$ and $O(\epsilon^2\delta^1)$, we obtain the equations

$$a \frac{d\mathcal{A}}{d\tau} = b\mathcal{A} + c\mathcal{A}|\mathcal{A}|^2 + d\mathcal{A}|\mathcal{B}|^2, \tag{3.9a}$$

$$a \frac{d\mathcal{B}}{d\tau} = b\mathcal{B} + c\mathcal{B}|\mathcal{B}|^2 + d\mathcal{B}|\mathcal{A}|^2, \tag{3.9b}$$

for the complex amplitudes \mathcal{A} and \mathcal{B} , correct to $O(\delta)$, of the leftward and rightward travelling waves, respectively. The complex coefficients a , b , c and d are given in the Appendix. The system (3.9) describes the nonlinear interaction between the two counter-propagating waves near a Hopf bifurcation point, and can be used to determine the stability, and relative stability, of the travelling and standing waves. The general form of these equations can be derived by considering the group of symmetries that characterize the physical system (e.g. Crawford & Knobloch 1991), and is known from other systems, such as a binary mixture in a porous medium (Knobloch 1986), thermosolutal convection (Deane, Knobloch & Toomre 1987), rotating Boussinesq convection (Knobloch & Silber 1990) and magnetoconvection (Matthews & Rucklidge 1993).

4. Results

4.1. Bifurcation structure

We shall analyse the amplitude equations (3.9) which represent an asymptotically exact model of the behaviour of the full system (2.12) near the primary Hopf bifurcation. We notice that, by representing the complex amplitudes \mathcal{A} and \mathcal{B} in terms of moduli and phases, the evolution equations for the moduli decouple from those for the phases if the amplitude equations (3.9) are first divided by the coefficient a (a is non-zero in the region of interest, see below). Generically, the moduli equations admit the following set of equilibrium solutions:

(i) conduction state:

$$(|\mathcal{A}|, |\mathcal{B}|) = (0, 0); \tag{4.1}$$

(ii) a pair of travelling waves:

$$(|\mathcal{A}|, |\mathcal{B}|) = (|\mathcal{A}^{TW}|, 0) \text{ or } (0, |\mathcal{A}^{TW}|), \text{ with } |\mathcal{A}^{TW}|^2 = -2\pi \frac{a_r}{|a|^2 \tilde{c}_r} R_2; \tag{4.2a, b}$$

(iii) standing waves:

$$(|\mathcal{A}|, |\mathcal{B}|) = (|\mathcal{A}^{SW}|, |\mathcal{A}^{SW}|), \text{ with } |\mathcal{A}^{SW}|^2 = -2\pi \frac{a_r}{|a|^2 (\tilde{c}_r + \tilde{d}_r)} R_2. \tag{4.3a, b}$$

Here, $\tilde{c} = c/a$, $\tilde{d} = d/a$, $R_2 = R_{20} + \delta R_{21}$, and the subscript r indicates the real part. Note that, in writing (4.2b) and (4.3b), we have made use of the linear relationship between a and b , given, correct to $O(\delta^0)$, by (A 1b) in the Appendix.

By analysing the linear stability properties of the solutions (4.2) and (4.3), we find that the travelling waves are stable if $\tilde{c}_r + \tilde{d}_r < 2\tilde{c}_r < 0$, and the standing waves are stable if $2\tilde{c}_r < \tilde{c}_r + \tilde{d}_r < 0$, given that the coefficient a_r is positive in the parametric region where the oscillatory convection is possible (see §4.2.2). The

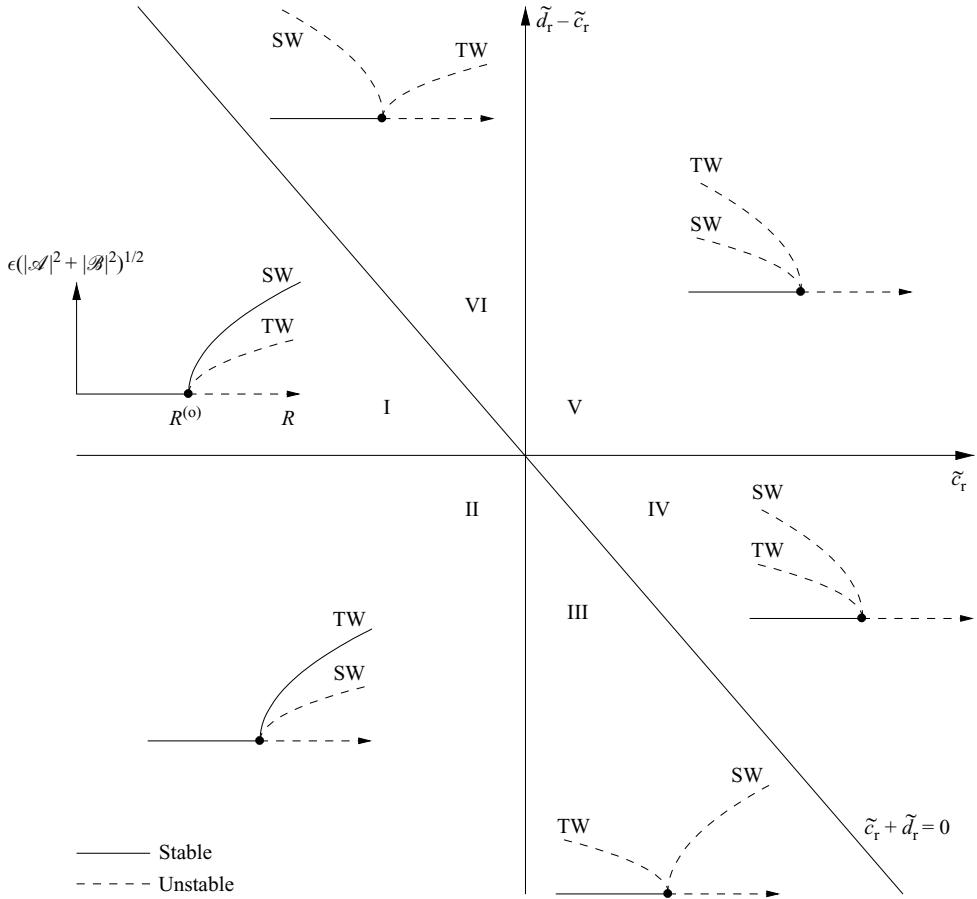


FIGURE 2. Bifurcation diagrams in the $(\tilde{c}_r, \tilde{d}_r - \tilde{c}_r)$ -plane, showing the equilibrated amplitude of the travelling waves (TW) and standing waves (SW), $\epsilon(|\mathcal{A}|^2 + |\mathcal{B}|^2)^{1/2}$, as a function of the Rayleigh number, R . Solid curves indicate (linearly) stable finite-amplitude oscillatory states, while dashed curves correspond to unstable oscillatory states. The $(\tilde{c}_r, \tilde{d}_r - \tilde{c}_r)$ -plane divides into six regions, I–VI, each characterized by the distinct branching behaviour and stability assignments of the two-dimensional primary oscillatory patterns. Note that the stable solutions can be identified in regions marked I and II, corresponding to the standing and travelling waves, respectively.

structure of the bifurcation diagrams and the stability properties of the equilibrium solutions (4.1)–(4.3), including the relative stability of the competing patterns, can be conveniently summarized in the $(\tilde{c}_r, \tilde{d}_r - \tilde{c}_r)$ -plane, as illustrated in figure 2. Note that both non-trivial solution branches, i.e. the left- and right-travelling waves, and the standing waves, bifurcate simultaneously at the linear Rayleigh number for the onset of oscillatory convection, $R = R^{(0)} \equiv R_{00} + \delta R_{01}$. The solid curves indicate (linearly) stable solution branches, and the dashed curves unstable ones. We see that stable solutions are present provided both travelling- and standing-wave branches bifurcate supercritically. In other words, it is not possible for a pattern to be stable when another one is subcritical. Furthermore, if both branches bifurcate supercritically, the stable solution is the one with the larger Nusselt number ($\sim 1 + \epsilon^2(|\mathcal{A}|^2 + |\mathcal{B}|^2)$). To investigate the eventual stabilization of the initially unstable subcritical branches of

either type at larger amplitudes requires delicate higher-order analysis, which is not attempted here.

4.2. Stability diagrams

The forgoing analysis has shown that either travelling or standing waves can be stable near onset, depending on the particular values of the complex coefficients in the amplitude equations (3.9). In the interest of establishing specific predictions for the mushy-layer system, we investigate the dependence of the stability assignments of the oscillatory patterns on the system control parameters \bar{S} , $\bar{\mathcal{C}}$, K_1 and K_2 . Even at leading order, $O(\delta^0)$, the coefficients are complicated functions of the system parameters, as well as the wavenumber k and the frequency ω_{01} . From now onwards we shall concentrate, for simplicity, only upon the leading-order results quoted in the Appendix.

In general, in order to assess the stability of travelling and standing waves properly, the coefficients in the amplitude equations have to be evaluated at a value of the wavenumber k that minimizes the Rayleigh number $R^{(0)}$ for the onset of the oscillatory instability. Nevertheless, by performing numerical computations for the linear stability problem (see equations (3.5*a, b*)), similar to those by Anderson & Worster (1996), it can be shown that the wavenumber that minimizes $R^{(0)}$ is only slightly greater than π , the critical wavenumber corresponding to the steady convective mode, over the parameter ranges where the oscillatory mode becomes unstable before the steady mode. This suggests that we can reduce the amount of calculation involved by fixing the wavenumber at $k = \pi$ (see §§4.2.2–4.2.4). A discussion of the stability results for the case when k is set to its optimum value is deferred to §4.2.5.

4.2.1. Stability considerations for steady convection

For $\omega_{01} = 0$, and in the limit of small K_1 , the solutions presented in §3 reduce to the results of the weakly nonlinear theory for steady mushy-layer convection in two dimensions given by Anderson & Worster (1995). They showed that a two-dimensional pattern of rolls is always supercritically bifurcating. Note that in the present analysis, in contrast, we have assumed that $K_1 = O(1)$ as $\delta \rightarrow 0$. It is natural to ask, therefore, whether the inclusion of the physical effect associated with leading-order, nonlinear permeability variations due to solid-fraction perturbations, measured by K_1 , would cause a change in the nature of the pitchfork bifurcation to rolls, by making steady convection more sensitive to the Darcy drag and thus altering the positive feedback required for a subcritical bifurcation. Indeed, by analysing the roll solution to the amplitude equation (3.9*a*), and using equations (A 1) and (A 2*a*) with ω_{01} set to zero, we find that it is now possible for steady roll convection to be subcritical when

$$\frac{K_1}{\Omega \bar{\mathcal{C}}} > \frac{\sqrt{3}}{32} \left[35 + 352 \frac{K_2}{(\Omega \bar{\mathcal{C}})^2} \right]^{1/2} - \frac{3}{32} \quad (4.4)$$

and supercritical otherwise. For the case $K_2 = 0$, we thus obtain subcritically bifurcating rolls if $K_1/(\Omega \bar{\mathcal{C}}) > \frac{1}{32}(\sqrt{105} - 3) \approx 0.226$ (cf. Amberg & Homsy 1993).

4.2.2. Stability considerations in the limiting case of $\omega_{01} \ll 1$

Before presenting the results of the full computations, we address a particular limiting case in which the pattern selection problem can be resolved explicitly. Specifically, since the oscillatory frequency ω_{01} , involved in the leading-order coefficients (A 1)–(A 3) of (3.9), has to be determined as the root of the transcendental equation (3.5*b*), it is, in general, not possible to give a simple criterion for the stability

of travelling and standing waves. We may, however, make some analytical progress by recognizing that close to the boundary in the parameter space where the Hopf bifurcation to travelling and standing waves coincides with the pitchfork bifurcation to steady convection, the frequency at the Hopf bifurcation is small. For simplicity, we confine our discussion of the limiting case $\omega_{01} \rightarrow 0$ to small values of K_1 , of $O(\delta)$ (cf. Riahi 2002), though the asymptotic results to follow can readily be generalized to $K_1 = O(1)$.

Expanding (3.5*b*), with k set equal to π , for small values of ω_{01} , we obtain

$$\pi^2 \left(\Omega - 2 \frac{\bar{S}}{\Omega \bar{\mathcal{C}}^2} \right) \omega_{01} + \frac{2}{3}(\pi^2 - 9) \frac{\bar{S}}{\Omega \bar{\mathcal{C}}^2} \omega_{01}^3 + O(\omega_{01}^5) = 0. \tag{4.5}$$

A first approximation to the non-trivial solution of (4.5) can be obtained by neglecting terms of $O(\omega_{01}^5)$. This yields

$$\omega_{01}^2 \sim \frac{3\pi^2}{\pi^2 - 9} \left[1 - \frac{1}{2} \frac{(\Omega \bar{\mathcal{C}})^2}{\bar{S}} \right]. \tag{4.6}$$

Note that the bifurcation to oscillatory convection occurs when ω_{01}^2 is positive, or, equivalently, when the coefficient a_r of the time derivative in the moduli equations, evaluated at $\omega_{01} = 0$, is negative (cf. Anderson & Worster 1995). Thus, in the range of interest $\bar{S}/(\Omega \bar{\mathcal{C}})^2 > \frac{1}{2}$ (see equation (4.6)). Note that, since we have taken $k = \pi$, the point at which ω_{01} vanishes corresponds to the appearance of the oscillatory mode at the minimum of the neutral stability curve for the real, rather than oscillatory, mode.

Recall that the stability assignments of the oscillatory solutions are determined by the signs of \tilde{c}_r , $\tilde{c}_r + \tilde{d}_r$ and $\tilde{d}_r - \tilde{c}_r$ (cf. figure 2). On performing the expansion, consistent with (4.6), of these expressions, and considering the signs of expressions thus obtained in the region $\bar{S}/(\Omega \bar{\mathcal{C}})^2 > \frac{1}{2}$, we find that the standing and travelling waves are stable when

$$\bar{Q}_1 < \frac{\bar{S}}{(\Omega \bar{\mathcal{C}})^2} < \bar{Q}_2, \quad \text{and} \quad \frac{\bar{S}}{(\Omega \bar{\mathcal{C}})^2} > \bar{Q}_2 \tag{4.7a, b}$$

respectively, where

$$\bar{Q}_1 = \frac{3\pi^2}{2(102\pi^4 - 569\pi^2 - 2048)} \left[16\pi^2 - 65 - 12(\pi^2 - 9) \frac{\bar{S}}{K_2} \right], \tag{4.8a}$$

$$\bar{Q}_2 = \frac{\pi^2}{2(2048 + 181\pi^2 - 30\pi^4)} \left[48\pi^2 - 121 - 12(\pi^2 - 9) \frac{\bar{S}}{K_2} \right]. \tag{4.8b}$$

It should be remarked that the criteria we have obtained are restricted by the condition $\omega_{01} \ll 1$, i.e by $\bar{S}/(\Omega \bar{\mathcal{C}})^2 \ll \frac{3}{2}\pi^2/(2\pi^2 + 9) \approx 0.515$.

Relations (4.7), along with (4.8), embody an important result from the viewpoint of the pattern selection problem and transitional behaviour between the stable oscillatory states. We note first that the presence of oscillatory convection in the mushy-layer model is controlled by the parameters \bar{S} and $\bar{\mathcal{C}}$ (or, in original, unscaled variables, by S , \mathcal{C} and δ), as can be deduced from (3.5*b*) or (4.6). Our asymptotic results reveal that a preference for distinct wave patterns, and hence the possibility of their realization in experiments, is dominated by a particular physical effect associated with nonlinear interaction between temperature and flow fields, represented by the terms proportional to \bar{S}/K_2 in (4.8). A relationship between these asymptotic stability criteria and the numerically determined stability results is discussed in the following section.

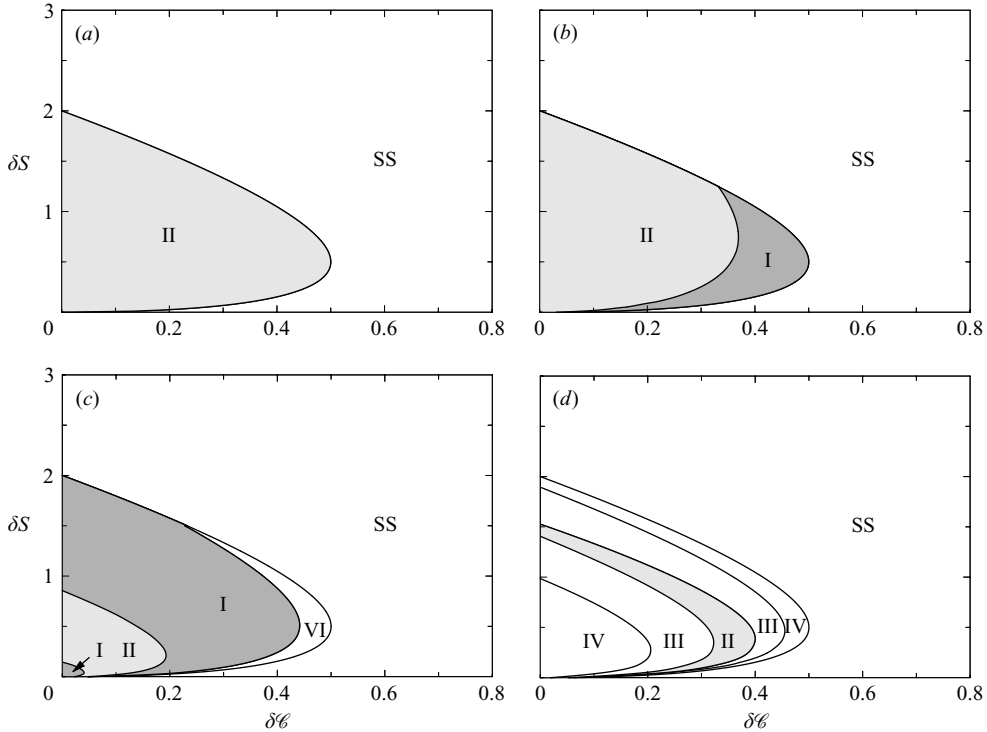


FIGURE 3. Stability regions in the $(\delta S, \delta \mathcal{C})$ -plane. A diagram showing the regions in the parameter space where various features of finite-amplitude two-dimensional convection can be identified. Steady states (SS), taking the form of rolls, are supercritically stable in (a)–(c), and subcritically unstable in (d). Inside the outermost solid curve in each of the plots, oscillatory solutions are located; this region can split into a number of portions, marked I–VI, in which distinct oscillatory branching behaviour can be identified (see figure 2). The light-shaded portion corresponds to those parameter values where stable travelling waves are predicted, while the dark-shaded portions indicate where stable standing waves are expected to appear. In the regions where either oscillatory bifurcation is subcritical (regions III–VI, cf. figure 2), our analysis does not determine the preferred behaviour. Four representative cases are shown: (a) $K_1 = 0, K_2 = 0$; (b) $K_1 = 0, K_2 = 0.05$; (c) $K_1 = 0, K_2 = 1$; (d) $K_1 = 3, K_2 = 6$.

4.2.3. Stability regions: $(\delta \mathcal{C}, \delta S)$ -space

In the general case of $\omega_{01} = O(1)$, the coefficients \tilde{c}_r and \tilde{d}_r were computed numerically in order to investigate whether travelling or standing waves are preferred close to the onset of oscillatory convection in mushy layers. We begin in figure 3 with a representation of the regions of stability in the parameter space spanned by \bar{S} and \mathcal{C} , for four representative sets of permeability coefficients K_1 and K_2 . For $\bar{S}/(\Omega \mathcal{C})^2 < \frac{1}{2}$, the convective instability is steady (see equation (4.6)), taking the form of two-dimensional rolls. From the criterion (4.4), we find that steady rolls in figures 3(a–c) bifurcate supercritically, while the roll branch bifurcates subcritically, and is thus unstable with respect to two-dimensional perturbations, on the scale of figure 3(d).

The region where $\bar{S}/(\Omega \mathcal{C})^2 > \frac{1}{2}$, lying to the left of the outermost solid curves in each of the plots in figure 3, divides into a number of portions, labelled I–VI, corresponding to distinct oscillatory branching behaviour as classified in figure 2. The regions with stable patterns are, in addition, shaded, with light and dark shading

corresponding to travelling and standing waves, respectively. Note that the two patterns cannot be stable simultaneously. We see that for the case $K_1=0$, $K_2=0$ (figure 3a), both oscillatory branches bifurcate supercritically (cf. figure 2), with the travelling waves being the stable pattern. The mushy-layer system behaves like a passive porous medium, i.e. convection is not affected by the deviations in the local growth of dendrites through the action of the Darcy drag forces. There is then no positive feedback mechanism in the system, which is required for a subcritical bifurcation.

For non-zero K_2 , with $K_1=0$, standing waves may be seen first as \mathcal{C} is decreased, depending on the value of \bar{S} (figure 3b). If standing waves are seen first, they are replaced by travelling waves as \mathcal{C} is decreased further. For $\omega_{01} \ll 1$, or, equivalently, close to the boundary between steady and oscillatory behaviour, the approximate location of the curve marking the transition between stable travelling and standing waves is given by $\bar{S}/(\Omega\mathcal{C})^2 = \bar{Q}_2$ from (4.7). We note that this transition appears only if $0 < K_2 \lesssim 12\pi^2(\pi^2 - 9)/(39\pi^4 - 151\pi^2 - 1024) \approx 0.080$. (The particular case of $K_1=0$, $K_2=0.05$ was also considered by Riahi (2002), who examined the limit of $K_1 \rightarrow 0$. Note, however, an incorrect identification of stability regions in figure 7 of his paper: when $\bar{S}/(\Omega\mathcal{C})^2 < \frac{1}{2}$, i.e. $G_t < \frac{1}{2}$ in his notation, an oscillatory instability is no longer present in the system.)

As K_2 increases further, with K_1 still fixed at zero, subcritical behaviour becomes discernible (figure 3c, region VI). From (4.7a), we find that standing waves may remain unstable until \mathcal{C} decreases to a curve given approximately by $\bar{S}/(\Omega\mathcal{C})^2 = \bar{Q}_1$ before gaining stability (with \bar{S} and δ fixed); near the boundary between the steady and oscillatory convection, this transition occurs if $0 < K_2 \lesssim 36\pi^2(\pi^2 - 9)/(1024 + 187\pi^2 - 27\pi^4) \approx 1.290$ (though it is not seen in figure 3b). The standing waves may lose stability to travelling waves as \mathcal{C} decreases, depending on the value of \bar{S} . As the origin of the $(\delta\mathcal{C}, \delta S)$ -plane is approached, stability is transferred back to standing waves; this result is limited, however, in that our asymptotic analysis requires both \mathcal{C} and \bar{S} to be $O(1)$. The situation depicted in figure 3(c) persists qualitatively for yet larger K_2 .

Figure 3(d) shows the case when the permeability of the mushy layer is sensitive to both the linear and quadratic variations in the local solid fraction. A representative case of $K_1=3$, $K_2=6$ is shown, corresponding to the constitutive relationship $\Pi = (1-\phi)^3$ adopted in many theoretical studies on convection in mushy layers (e.g. Fowler 1985; Worster 1992; Schulze & Worster 1999). Depending on the selected value of \bar{S} , our calculations reveal the presence of an interval of stable travelling waves. Throughout the rest of the oscillatory region, at least one of the primary branches is subcritical (regions III and IV). Recall that in the regions where either oscillatory bifurcation is subcritical, our analysis cannot determine the preferred behaviour near onset.

4.2.4. Stability regions: (K_1, K_2) -space

One of the most important aspects of figure 3 is that the stability of the primary oscillatory branches is controlled primarily by the permeability coefficients K_1 and K_2 , although the presence of the oscillatory instability is determined solely by the Stefan number S , compositional ratio \mathcal{C} and the mushy-layer thickness δ . In order to examine the stability for a wider range of possible morphologies of the solid dendrites, reflected in the particular values of K_1 and K_2 , we show in figure 4 the stability boundaries in the (K_1, K_2) -plane for four illustrative cases of fixed \bar{S} and \mathcal{C} .

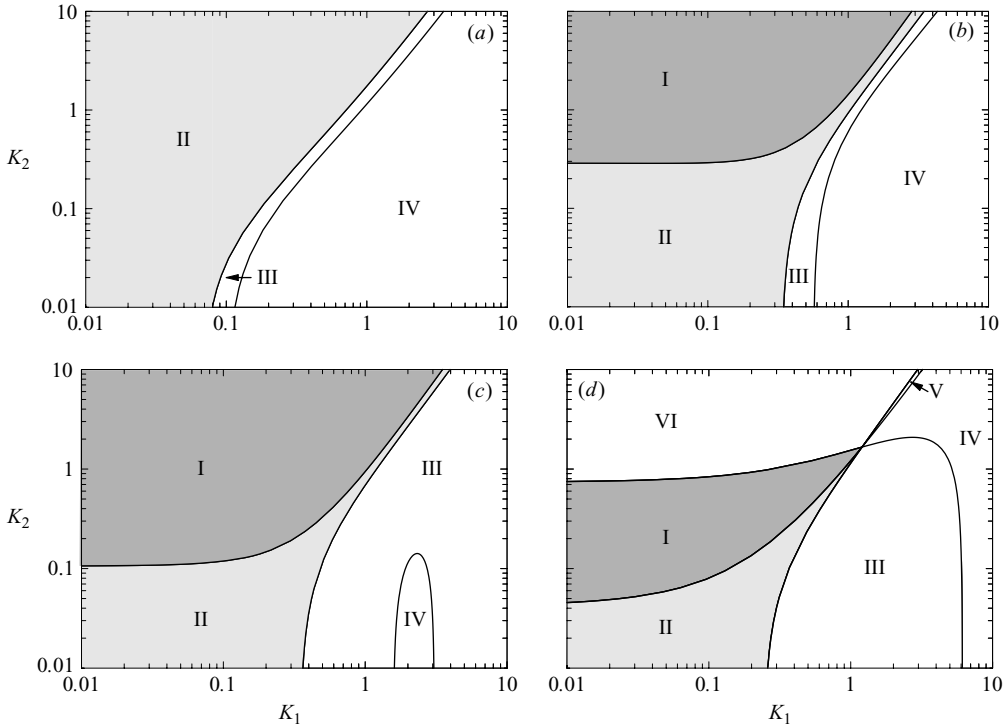


FIGURE 4. Stability regions in the (K_1, K_2) -plane. Four illustrative cases are shown: (a) $\bar{S} = 0.1$, $\bar{\mathcal{C}} = 0.05$; (b) $\bar{S} = 1$, $\bar{\mathcal{C}} = 0.05$; (c) $\bar{S} = 1$, $\bar{\mathcal{C}} = 0.2$; (d) $\bar{S} = 1$, $\bar{\mathcal{C}} = 0.4$. Note that for each set of \bar{S} and $\bar{\mathcal{C}}$ the oscillatory instability is possible (cf. figure 3). The light-shaded and dark-shaded portions correspond to those parameter values for which stable travelling and standing waves are predicted, respectively. Also note that the presence of the oscillatory convective modes, unlike their stability, is not controlled by the permeability coefficients K_1 and K_2 .

Note that for each set of \bar{S} and $\bar{\mathcal{C}}$ considered, the oscillatory instability is possible (cf. figure 3).

For smaller values of \bar{S} and $\bar{\mathcal{C}}$ (figure 4a), the travelling waves are found to be the only stable pattern, existing for any K_2 . For larger \bar{S} , with $\bar{\mathcal{C}}$ kept fixed, the travelling waves give way to stable standing waves as K_2 increases (figure 4b). In both cases note the appearance of an unbounded domain in which both oscillatory branches are subcritical (region IV), separated from the region with the stable travelling waves by a relatively narrow region in which subcritical travelling waves and (unstable) supercritical standing waves coexist (region III).

For moderate values of \bar{S} and $\bar{\mathcal{C}}$ (figure 4c), the travelling waves lose stability to standing waves at slightly lower values of K_2 compared with figure 4(b), and the region in which subcritical, and hence unstable, travelling and standing waves are found is left bounded (cf. figure 4b). With increasing $\bar{\mathcal{C}}$ (figure 4d), we find that the regions of stable oscillatory patterns become bounded. If K_1 is sufficiently small, the travelling waves may lose stability and the standing waves become the preferred pattern. The standing waves can lose stability again as K_2 is increased further, leaving a region with no stable primary pattern (region VI). Note that all the genuine bifurcation structures, itemized in figure 2, can be realized in the mushy-layer system in this particular case.

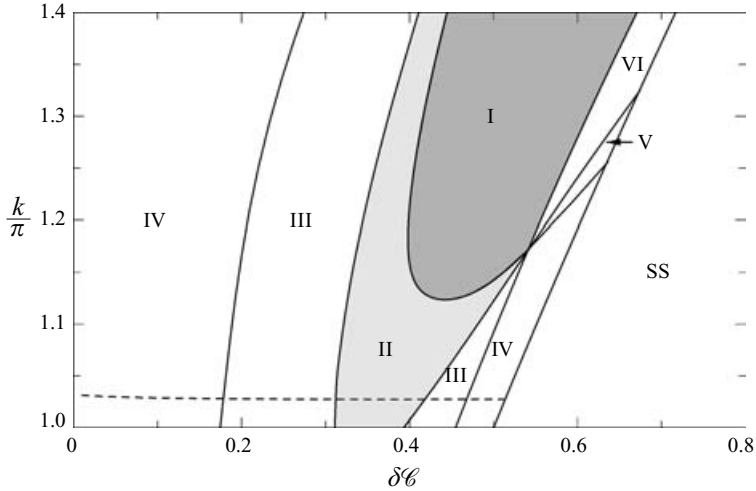


FIGURE 5. Stability regions in the $(\delta\mathcal{C}, k/\pi)$ -plane for fixed $\bar{S}=0.5$, $K_1=3$ and $K_2=6$. Notice that a slice through $k=\pi$ corresponds to a slice through $\bar{S}=0.5$ in figure 3(d). In the region labelled SS, the steady rolls are subcritically bifurcating, and thus unstable. The oscillatory flows in the form of travelling waves and standing waves are stable in the light-shaded and dark-shaded regions, respectively. Also shown is the wavenumber minimizing the linear Rayleigh number for the onset of oscillatory convection (dashed curve); the critical wavenumber for the onset of steady roll convection is equal to π .

4.2.5. Stability regions: $(\delta\mathcal{C}, k/\pi)$ -space

The calculations described above were all performed at the externally imposed wavenumber, $k=\pi$, rather than at a value that would minimize the Rayleigh number for the onset of the oscillatory mode of instability. In order to appreciate the significance in the pattern selection process of the optimum value of the wavenumber, we show in figure 5 the stability boundaries as functions of the compositional ratio \mathcal{C} and the scaled wavenumber k/π with fixed $\bar{S}=0.5$, $K_1=3$ and $K_2=6$. In figure 3(d) a slice through $\bar{S}=0.5$ corresponds to a slice through $k/\pi=1$ in figure 5. The critical value of the wavenumber as a function of \mathcal{C} is indicated by a dashed curve. We see that this variation is rather weak, leading to the same sequence of transitions on increasing \mathcal{C} as for $k=\pi$ (cf. figure 3d). We expect, therefore, that the value $k=\pi$ which we have chosen to display the stability results in the previous sections is representative of the results which would involve the optimum k . It is also interesting to note that a parameter range in which the supercritical Hopf bifurcation gives rise to stable travelling waves is slightly larger than in the case of $k=\pi$.

Often, numerical experiments are carried out at a fixed value of the wavenumber. Hence, in figure 5, the stability regions are given also for a wavenumber greater than the critical one. We observe that the stability properties of the oscillatory patterns can be profoundly affected by the choice of k . In particular, travelling waves are the only stable pattern favoured for smaller values of k ($\pi \lesssim k \lesssim 1.117\pi$). At intermediate k ($1.117\pi \lesssim k \lesssim 1.172\pi$), the travelling waves lose stability to standing waves as \mathcal{C} increases; but they acquire it again on increasing \mathcal{C} yet further. For larger k ($k \gtrsim 1.172\pi$), the stable travelling waves are superseded by stable standing waves with increasing \mathcal{C} . It is important to note that, with increasing k , the region where the oscillatory instability is possible increases, with the portion in which the stable standing waves are preferred gradually getting larger. Thus, if experimental control

can be enforced on the size of convection cells, the oscillatory flows in the form of standing waves can be exhibited by mushy-layer systems with much larger values of the compositional ratio \mathcal{C} than expected from the linear theory (cf. Anderson & Worster 1996).

4.2.6. *Nonlinear detuning*

At a Hopf bifurcation, the frequency of the travelling and standing waves is, correct to $O(\epsilon^0 \delta^1)$, $\omega = \delta\omega_{01}$. In the nonlinear regime, the frequencies of the oscillatory convecting states may differ from those predicted by the linear theory (see equation (3.1e)). Analysing the time-independent solutions to phase equations derived from (3.9), we obtain

$$\omega = \delta\omega_{01} + \epsilon^2 \omega_2^{\text{TW}} = \delta\omega_{01} + \frac{c_i}{a_r} (\epsilon |\mathcal{A}^{\text{TW}}|)^2, \tag{4.9a}$$

$$\omega = \delta\omega_{01} + \epsilon^2 \omega_2^{\text{SW}} = \delta\omega_{01} + \frac{c_i + d_i}{a_r} (\epsilon |\mathcal{A}^{\text{SW}}|)^2, \tag{4.9b}$$

for the frequency of the travelling and standing waves, respectively, in the neighbourhood of the Hopf bifurcation point. Here, the subscript i indicates the imaginary part. Since a_r is always positive over the parameter space where the oscillatory states are possible, it follows from (4.9) that the nature of the nonlinear detuning is determined by the signs of c_i and $c_i + d_i$. Here, we examine this issue asymptotically in the limit $\omega_{01} \rightarrow 0$, capturing the portion of (\mathcal{C}, \bar{S}) -parameter space close to the boundary between the oscillatory and steady behaviours. Considering the dominant behaviour as $\omega_{01} \rightarrow 0$, we find a critical value of K_2 ,

$$K_2 = \frac{23}{16} K_1^2, \tag{4.10}$$

below which the frequency of the travelling waves increases with amplitude and above which it decreases. In a similar way, for the standing waves we find

$$K_2 = \frac{1}{36\pi^2 - 64} [(45\pi^2 - 244)K_1^2 + 9\pi^2 \Omega \bar{\mathcal{C}} K_1]; \tag{4.11}$$

now, however, the frequency of standing waves decreases with amplitude for K_2 smaller than this critical value and increases for greater values.

These results can be discussed in the light of the stable oscillatory solutions identified in the (\mathcal{C}, \bar{S}) -parameter space at selected values of K_1 and K_2 (see figure 3). For instance, we deduce that the stable, finite-amplitude travelling waves predicted to occur when $K_1 = 3$, $K_2 = 6$ (see region II in figure 3d) will propagate at a phase velocity slightly greater than that determined by the linearized theory, provided the values of \bar{S} and \mathcal{C} lie close to the boundary between the steady and oscillatory behaviours.

4.3. *Structure of nonlinear oscillatory convection*

We now examine the structure of the finite-amplitude oscillatory solutions. We consider the two representative sets of the system control parameters which give rise to the appearance of supercritical, and hence stable, oscillatory convection in the form of travelling and standing waves respectively. For each parameter regime, we start with a summary of linear theory, without which the nonlinear results would be incomprehensible. Although dominated by the eigensolutions of the linear problem, convective oscillatory solutions at finite amplitude reveal several unexpected features that have a particular bearing on the structural development of the resulting eutectic solid.

4.3.1. Travelling waves

We consider first the travelling-wave solution, for $\bar{S} = 0.5$, $\bar{\mathcal{C}} = 0.35$, $K_1 = 3$, $K_2 = 6$, and $\delta = 0.1$. Accordingly, the solution corresponds to a supercritically bifurcating convective state (cf. figure 3*d*). We take $k = \pi$, and focus on the left-travelling waves only. The perturbation amplitude ϵ is fixed at ≈ 0.014 , this being close to a critical value for breakdown of the model (an incipient, supercritical chimney formation; see figure 6*c*). At these parameters, $R^{(0)} \approx 5.145$, $\omega_{01} \approx 1.064\pi$ and $\omega_{20}^{\text{TW}} \approx -182.843\pi$.

Linear theory (Anderson & Worster 1996), together with the basic-state solution (2.11) and the leading-order infinitesimal perturbations (3.3*a–d*), shows that at any instant in time the spatial structure of the thermal and flow fields is identical to that of the steady state. In particular, the flow field corresponds to convection in the form of two-dimensional rolls with axes in the y -direction. The thermal fluctuations, induced by the convective motion, lag behind the flow pattern as it translates horizontally, with the vertical motion being aligned with cold rising fluid depleted of solute, and hot falling fluid enriched in solute. The leading-order structure of the solid fraction, however, differs from its steady-state equivalent: in the steady state, the perturbations to the solid fraction lead to the formation of channels of reduced solid fraction which are vertically oriented, but in oscillatory convection the slope of the solid-fraction channels is, in general, non-monotonic. In consequence, solid-fraction channels, being potential seed locations for chimney formation, occur principally in the roll centres, rather than coinciding with the horizontal positions where the upward flow takes its maximum. An account of quantification of these issues in terms of ω_{01} is given in Anderson & Worster (1996).

We now turn to discussing the properties of the travelling-wave solution in the nonlinear regime. Figure 6 shows a snapshot of the fields in the (\bar{x}, \bar{z}) -plane at $\bar{t} = 0$. Note that the fields are still time-periodic, though the wave pattern is translated at a phase speed $\omega/k \approx 0.069$ which is less than that determined by the linear theory. In contrast to the marginal case, the boundaries between adjacent cells are no longer vertical (figure 6*a*): the cell boundary at which the flow is upwards leads at the top and lags at the bottom, while the opposite is true for the cell boundary at which the flow is downwards. Mathematically, this trapezoidal appearance of the travelling-wave convection can be ascribed to the $O(\epsilon^2\delta^0)$ flow-field correction which effectively makes a phase of the flow field \bar{z} -dependent. Note that this correction is, in general, proportional to $|\mathcal{A}|^2 - |\mathcal{B}|^2$; thus it is present for a travelling wave but not for a standing wave (cf. §4.3.2). Physically, this structure reflects the spatial adjustment of the flow field to the leading-order non-vertical solid-fraction channels, occurring at $O(\epsilon^2\delta^0)$. It is also important to note that the presence of this effect is associated with the nonlinear variations of the permeability with the perturbations to the basic-state solid fraction: this physical effect would not have been identified had we taken $K_1 = O(\delta)$ rather than $K_1 = O(1)$.

The disturbance of the thermal field is remarkably weak, with $|\epsilon\hat{\theta}|$ attaining at most 2% of the absolute maximum base-state value, perhaps emphasizing the importance of compositional effects over the thermal ones in controlling the convective dynamics of the system. Therefore, in figure 6(*b*), we have chosen to show the thermal perturbation, $\epsilon\hat{\theta}$, rather than the total thermal field. The upward motion is associated with negative thermal fluctuations in the bulk of the mushy layer. This correlation is expected since, even in this weakly nonlinear regime, compositional buoyancy for the upward motion is still provided by the negative solutal perturbation.

The spatial structure of the solid-fraction field, shown in figure 6(*c*), is dominated by the marginal solid-fraction distribution described above, confirming the presence

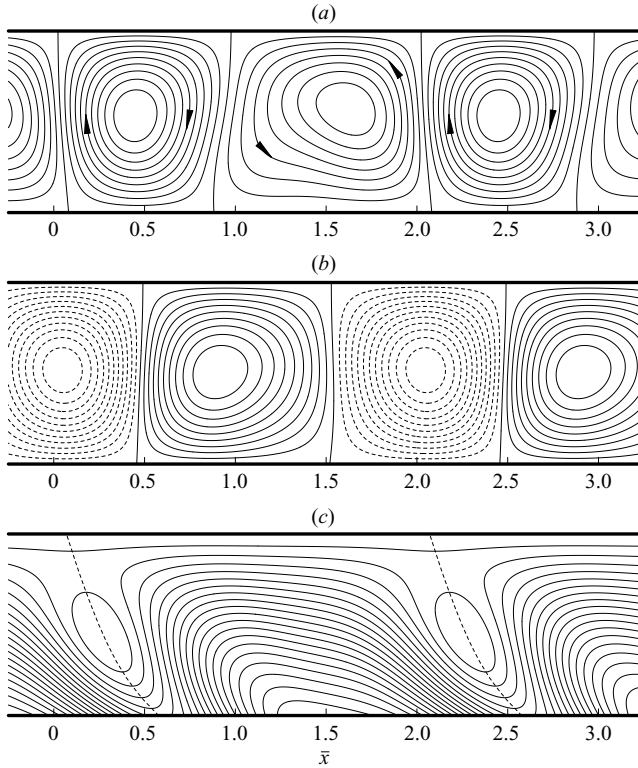


FIGURE 6. Nonlinear stable travelling waves for $\bar{S} = 0.5$, $\bar{\mathcal{C}} = 0.35$, $K_1 = 3$, $K_2 = 6$, $\delta = 0.1$ and $\epsilon \approx 0.014$. A snapshot of (a) stream function, (b) perturbation temperature, and (c) solid fraction in the (\bar{x}, \bar{z}) -plane at $\bar{t} = 0$. For the stream function and perturbation temperature the contours quantify 0.1 of the corresponding extreme values, and for the solid fraction 0.05 of the maximum. The maximum values attained by the contoured quantities in (a), (b) and (c) are 0.552, 0.015 and 0.412, respectively. In (b), dashed contours indicate negative thermal fluctuations. The nonlinear perturbations lead to channels of reduced solid fraction, indicated by the dashed curves in (c). The wave pattern propagates towards the left as the mushy layer advances upwards.

of a phase lag between the dissolution caused by the flow and the overall solidification caused by pulling (Anderson & Worster 1996). Close inspection shows, however, that point symmetry of the solid-fraction perturbation about the trace of the solid-fraction channel, which is present in the linear case, is broken, as indicated by the lopsided contours in the regions where the solid fraction attains its peak values. The loss of symmetry in the nonlinear regime is a result of the additional heat that is transferred from the upper regions of the mush through the advection of the marginal temperature profile by the leading-order flow field, which tends, though lagging in time, to inhibit growth of the solid phase. Curiously, in this supercritical regime, the solid fraction drops to zero at some point along the solid-fraction channel, suggesting that the formation of chimneys in the mushy layers may not be an exclusively subcritical phenomenon.

The development of spatial asymmetry in the local solid fraction has important implications for the compositional structure in the resulting eutectic solid. The dimensionless bulk composition in the mushy region is defined as $\bar{\Theta} = (1 - \phi)\theta + \mathcal{C}\phi$,

which on evaluating at the solid–mush interface reduces to

$$\bar{\Theta}(\bar{x}, \bar{z} = 0, \bar{t}) = \epsilon(1 + \mathcal{C})\hat{\phi}(\bar{x}, \bar{z} = 0, \bar{t}). \quad (4.12)$$

This expression, describing the evolution of the local bulk composition in the eutectic solid, is plotted in figure 8(a), below, for the same parameter values as used for figure 6. As expected, the eutectic structure displays tilted behaviour, resulting from the vertical pulling of the solid and the horizontal propagation of the travelling-wave pattern, with the slope of the bulk-composition contours slightly larger than that determined from the linear theory. For a fixed \bar{t} , corresponding to a horizontal slice through the solid, the bulk composition exhibits purely sinusoidal variation in the horizontal at the marginal stability limit. In the nonlinear regime, however, the bulk composition rises more rapidly than it falls, so that the troughs are sharper than the peaks, as can be seen in figure 8(a) (cf. the spatially asymmetric pattern of behaviour in figure 6c). Note that the regions where the bulk composition is locally decreased below its basic-state zero value are a consequence of the upward flow which brings relatively depleted fluid that causes dissolution of dendrites.

4.3.2. Standing waves

To investigate the development of standing-wave convection, we studied the finite-amplitude solutions for $\bar{S} = 1$, $\mathcal{C} = 0.2$, $K_1 = 1$, $K_2 = 1$, and $\delta = 0.1$. Then the bifurcation is supercritical and the standing waves are stable (cf. figure 4c) in the neighbourhood of $R^{(o)} \approx 3.277$. Again, ϵ is fixed at a maximum allowed value for the validity of the model; $\epsilon \approx 0.022$. At these parameter values, $\omega_{01} \approx 1.069\pi$ and $\omega_{20}^{SW} \approx -3.443\pi$, so that the period of standing waves is $\bar{T} = 2\pi/\omega \approx 18.993$.

We shall focus first on describing standing waves at onset, thus completing the analysis of the structure of leading-order oscillatory modes commenced by Anderson & Worster (1996). Initially, the roll motion in a particular convection cell is clockwise, say, and the velocity is at a maximum. As the oscillation proceeds, the flow field falls off, drops to zero at $\bar{t} = \frac{1}{4}\bar{T}$ so that the motion becomes anticlockwise, and reaches its maximum again at $\bar{t} = \frac{1}{2}\bar{T}$. The behaviour during the second half of the cycle follows in an obvious manner. Note that, in contrast to the pattern for the travelling-wave mode, the rolls reverse direction without shifting their positions in the horizontal. The thermal-field perturbation is temporally in phase with the flow field as the mushy layer advances, with the same spatial correlation as in the steady case described above, as might be expected. The discussion of the time-evolution of the solid-fraction field is rendered somewhat more difficult. At any instant in time, the propensity for chimney formation is highest at every cell boundary, and so the leading-order solid-fraction channels are always aligned with the vertical and remain fixed in the horizontal. In addition, depending on the value of ω_{01} the channels may be continuous or they may appear divided, temporarily, into a number of vertical sections, their extents being periodic functions of time. Also note that, because the solid-fraction perturbations at the boundaries of a convection cell are out of phase in time, the channels appear to grow at the expense of each other.

Much of this rich behaviour carries over into the nonlinear regime. Figure 7 shows the spatial structure of the fields at five successive stages during half of a full cycle. Note that the cell boundaries are still vertical (see figure 7a), but owing to a \bar{z} -dependent temporal phase shift of the nonlinear flow-field corrections, there is no instant in time at which the cells are completely at rest. This is reflected by the appearance of relatively weak vertically stacked countercells during the flow reversal.

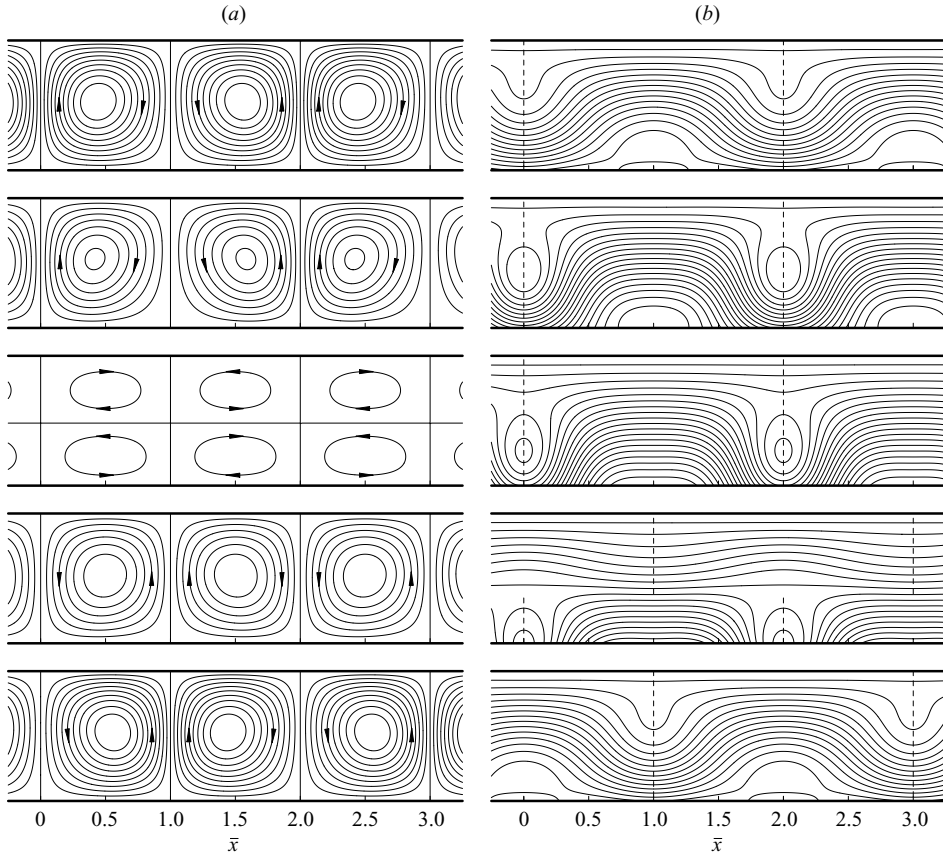


FIGURE 7. Nonlinear stable standing waves for $\bar{S}=1$, $\bar{C}=0.2$, $K_1=1$, $K_2=1$, $\delta=0.1$ and $\epsilon \approx 0.022$. Contours of (a) stream function and (b) local solid fraction in the (\bar{x}, \bar{z}) -plane at five equally spaced instants in time during a half-cycle, starting from the top. For the stream function the contours quantify 0.1 of the maximum, 0.602, attained at $\bar{t}=0$; the contour levels remain fixed throughout the sequence apart from the third instant, where the contours quantify 0.01 of the maximum. The solid-fraction contours quantify 0.05 of the maximum, 0.703, attained at $\bar{t}=\frac{1}{4}T$; the contours remain fixed throughout the sequence. The solid-fraction channels (dashed lines) are vertically oriented, and may appear at both boundaries of a convection cell, though their vertical extents vary in time. See text for a more complete description of this variation.

This pattern of behaviour is similar to that found by Schöpf & Zimmermann (1990) in the context of small-amplitude standing-wave convection in binary fluid mixtures with no-slip boundary conditions, although the underlying physical mechanism is, of course, different. Here, it is the presence of the leading-order non-uniformity in the permeability, measured by K_1 , which is responsible for this feature of the flow.

The development of the solid-fraction field is shown in figure 7(b), with the corresponding behaviour of the bulk composition in the eutectic solid displayed in figure 8(b). The solid fraction oscillates in much the same as the leading-order eigenfunction of the linear problem, though, interestingly, with a slight preference for the negative perturbations at the bottom of the mush. Notice also that, because the nonlinear solid-fraction field is approximately out of phase in time with the thermal

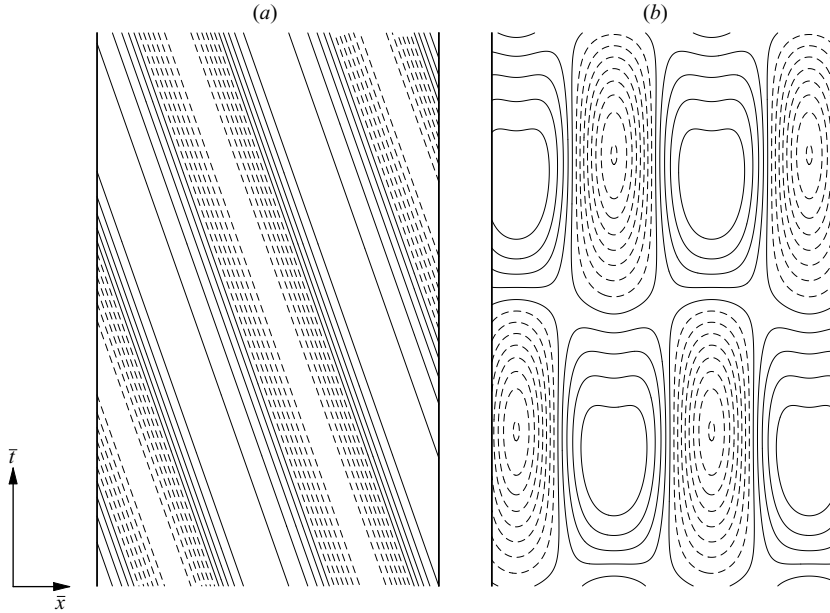


FIGURE 8. A space-time plot illustrating the stable oscillatory morphologies of the eutectic solid produced by the mushy-layer convection in the form of (a) travelling waves and (b) standing waves. Contours of the local bulk composition in the eutectic solid, obtained from (4.12), shown in (a) and (b) for the same parameter values as used in figures 6 and 7 respectively. The spatial scale spans the same range as the horizontal scale in figures 6 and 7. The timescale ranges over half a complete cycle, starting at $\bar{t}=0$. Note, however, the different scales for \bar{t} in (a) and (b), as the periods of oscillatory solutions are different (28.780 and 18.993, respectively). Note also that the dimensionless time \bar{t} can be regarded as the dimensionless height of the solid just formed. In both (a) and (b), the contours quantify 0.1 of the maximum, and dashed contours have negative values. The maximum values attained by $\bar{\theta}$ in (a) and (b) are 0.617 and 0.623 respectively.

and flow fields, the maximum amount of solid phase coincides with the moment when the motion is almost halted and the thermal fluctuations are least.

5. Conclusions

We have studied the nonlinear development of two-dimensional oscillatory convection in a mushy layer during binary alloy solidification. We performed a weakly nonlinear stability analysis that extends the linear theory of Anderson & Worster (1996) to the nonlinear regime. A key result of our analysis is a set of complex amplitude equations which describe the evolution and stability of finite-amplitude oscillatory convecting states in the vicinity of the (primary) Hopf bifurcation. By analysing these equations, we have identified oscillatory solutions in the form of travelling waves and standing waves, and determined the stability of each, and their relative stability.

Our analysis of the oscillatory solution branches shows that either travelling waves or standing waves can be (supercritically) stable, and thus preferred near the onset of oscillatory convection. We find that a preference for distinct wave patterns, and hence the possibility of their physical realization in the experiments, is determined predominantly by a particular choice of the permeability coefficients K_1 and K_2 , as

indicated in figure 4. Our analysis thus emphasizes the importance of a specific form of the constitutive relationship, relating the permeability to the local solid fraction, in selecting the pattern of the oscillatory convection in mushy layers. Moreover, the oscillatory solution that is stable has the greater value of the Nusselt number, and is thus more efficient at transporting solute in the system.

We have also demonstrated a possibility of subcritical oscillatory behaviour in mushy layers. We have found that the appearance of the subcritical Hopf bifurcation hinges on a single physical effect associated with the leading-order non-uniformity in the permeability due to the basic-state solid fraction and its perturbations. This bifurcation cannot occur unless we consider a parameter regime which has $K_1/(\delta\mathcal{C}) = O(1)$. It is interesting to note that the same nonlinear effect was responsible for the appearance of the subcritical pitchfork bifurcation to the steady two-dimensional roll solution in the analysis of Amberg & Homsy (1993). The subcritical Hopf bifurcation in the present analysis gives rise to travelling-wave and standing-wave solutions which are initially unstable (see figure 2). At larger amplitudes, these solutions can acquire stability at the turning points associated with the saddle-node bifurcations along the primary oscillatory branches; to follow this would demand a higher-order analysis with an enhanced computing requirement.

We have also analysed the nonlinear structure and dynamics of oscillatory convection. For instance, the results in §4 suggest that, despite inferences from linear theory, the travelling-wave convection favours spatially asymmetrical cells in the nonlinear regime (see figure 6). A physical explanation of this was given in §4. We point out that a particular parameter regime, namely that in which $K_1/(\delta\mathcal{C}) = O(1)$ so that the dominant non-uniformities in the permeability due to the basic-state solid fraction and its perturbations are captured, is an important feature here.

The analysis presented in this paper has in part been motivated by the recent experimental observations of Solomon & Hartley (1998). They performed experiments on an aqueous solution of ammonium chloride and, by direct measurement of the temperature field in the growing mushy layers, were indeed able to observe periodic convective behaviour. Although intriguing in the light of the oscillatory instability studied here, the sense of the flow did not cyclically reverse as the pattern evolved, indicating that the observed behaviour may not be directly related to the standing-wave pattern examined in our study. Instead, we anticipate that the periodic pattern observed in their experiments arises from an intricate nonlinear interaction between steady and oscillatory convecting states. An important extension of this study will thus be to treat the behaviour of the mushy-layer system close to the situation where the primary Hopf bifurcation coincides with the pitchfork bifurcation to steady convection (a Takens–Bogdanov bifurcation). This multiple bifurcation deserves particular attention partly because of its potential relevance to the vacillatory motion seen by Solomon & Hartley (1998), and partly because typically the behaviour identified near such a bifurcation persists for parameter values substantially different from their critical values. Finally, it would be of general interest to consider three-dimensional oscillatory patterns, and to determine their stability and competition with the two-dimensional oscillatory states studied here. The present study forms a basis for future investigation of these challenging problems.

This research was supported by a Royal Society/NATO Postdoctoral Fellowship held by P.G. The authors would like to thank D.M. Anderson for helpful comments on an earlier draft of this paper and J.H.P. Dawes for helpful discussions.

Appendix. Coefficients of the amplitude equations

A purpose of the appendix is to provide expressions for the complex coefficients a , b , c and d appearing in the amplitude equations (3.9), with the particular goal of displaying the explicit dependence of the coefficients on the system control parameters (or combinations thereof). Here, we concentrate upon the leading-order results, i.e. on writing $a = a_0 + \delta a_1$, and similarly for b , c and d , terms a_1 , b_1 , c_1 and d_1 which make small, of $O(\delta^1)$, corrections are not recorded.

The coefficients of the linear terms of the amplitude equations (3.9) take the form

$$a_0 = \frac{\pi}{k}\Omega + \frac{\pi(\pi^2 + k^2)}{k(\pi^2 - \omega_{01}^2)} \left[\frac{\pi^2 + \omega_{01}^2 - 2\pi^2 e^{-i\omega_{01}}}{\pi^2 - \omega_{01}^2} - \frac{8i\pi^2 \omega_{01}(1 + e^{-i\omega_{01}})}{(\pi^2 - \omega_{01}^2)^2} \right] \frac{\bar{S}}{\Omega \bar{\mathcal{E}}^2}, \quad (\text{A } 1a)$$

$$b_0 = 2\pi R_{20} - ia_0 \omega_{20}. \quad (\text{A } 1b)$$

After a fair amount of algebra, we find that the coefficients of the nonlinear terms in (3.9) are given by

$$c_0 = -\frac{\pi}{2k}(\pi^2 + k^2)^2 + f_c(k) \frac{K_1}{\Omega \bar{\mathcal{E}}} + g_c(k, \omega_{01}) \left(\frac{K_1}{\Omega \bar{\mathcal{E}}} \right)^2 + h_c(k, \omega_{01}) \frac{K_2}{(\Omega \bar{\mathcal{E}})^2}, \quad (\text{A } 2a)$$

$$d_0 = -\frac{\pi}{k}(\pi^2 + k^2)^2 + f_d(k, \omega_{01}) \frac{K_1}{\Omega \bar{\mathcal{E}}} + g_d(k, \omega_{01}) \left(\frac{K_1}{\Omega \bar{\mathcal{E}}} \right)^2 + h_d(k, \omega_{01}) \frac{K_2}{(\Omega \bar{\mathcal{E}})^2}, \quad (\text{A } 2b)$$

where

$$f_c = \frac{\pi}{2k}(\pi^2 + k^2)(\pi^2 + 3k^2), \quad (\text{A } 3a)$$

$$f_d = \frac{\pi(\pi^2 + k^2)}{2k(\pi^2 - \omega_{01}^2)} \left[4\pi^2 k^2 - (\pi^2 + 3k^2)\omega_{01}^2 + \frac{i\pi^4(\pi^2 + k^2 - 2\omega_{01}^2)(e^{-2i\omega_{01}} - 1)}{\omega_{01}(\pi^2 - \omega_{01}^2)} \right], \quad (\text{A } 3b)$$

$$h_c = \frac{\pi(\pi^2 + k^2)^2}{k(\pi^2 - \omega_{01}^2)^2} \left[-\frac{64\pi^4 \omega_{01}^3 \sin \omega_{01} + (\pi^2 + k^2)(99\pi^6 - 83\pi^4 \omega_{01}^2 - 19\pi^2 \omega_{01}^4 + 3\omega_{01}^6)}{4(\pi^2 - \omega_{01}^2)(9\pi^2 - \omega_{01}^2)} \right. \\ \left. - \frac{i\pi^4[-9\pi^2(k^2 - \pi^2) + (13\pi^2 + 33k^2)\omega_{01}^2 + 2\omega_{01}^4]}{2\omega_{01}(\pi^2 - \omega_{01}^2)(9\pi^2 - \omega_{01}^2)} \right. \\ \left. - \frac{8i\pi^4 \omega_{01}[(5\pi^2 + 4k^2)e^{i\omega_{01}} - (3\pi^2 + 2k^2)e^{-i\omega_{01}}]}{(\pi^2 - \omega_{01}^2)(9\pi^2 - \omega_{01}^2)} - \frac{i\pi^4(k^2 - \pi^2 + 2\omega_{01}^2)e^{-2i\omega_{01}}}{2\omega_{01}(\pi^2 - \omega_{01}^2)} \right], \quad (\text{A } 3c)$$

$$h_d = \frac{\pi(\pi^2 + k^2)^2}{k(\pi^2 - \omega_{01}^2)^2} \left[-\frac{\pi^2}{2}(3\pi^2 + 11k^2) - \frac{1}{2}(3k^2 - \pi^2)\omega_{01}^2 \right. \\ \left. + \frac{i\pi^4[9\pi^2(\pi^2 + k^2) - (33k^2 - 13\pi^2)\omega_{01}^2 + 2\omega_{01}^4]}{\omega_{01}(\pi^2 - \omega_{01}^2)(9\pi^2 - \omega_{01}^2)} \right. \\ \left. - \frac{32i\pi^4 \omega_{01}[2k^2 e^{i\omega_{01}} - (\pi^2 + k^2)e^{-i\omega_{01}}]}{(\pi^2 - \omega_{01}^2)(9\pi^2 - \omega_{01}^2)} - \frac{i\pi^4(\pi^2 + k^2 - 2\omega_{01}^2)e^{-2i\omega_{01}}}{\omega_{01}(\pi^2 - \omega_{01}^2)} \right]. \quad (\text{A } 3d)$$

Expressions for g_c and g_d are of sufficient complexity that little insight would be gained by displaying them here. These extensive forms can be made available on request from the authors or the JFM editorial office.

REFERENCES

- AHARONOV, E., SPIEGELMAN, M. & KELEMEN, P. B. 1997 Three-dimensional flow and reaction in porous media: Implications for the Earth's mantle and sedimentary basins. *J. Geophys. Res.* **102**, 14821–14833.
- AMBERG, G. & HOMS, G. M. 1993 Nonlinear analysis of buoyant convection in binary solidification with application to channel formation. *J. Fluid Mech.* **252**, 79–98.
- ANDERSON, D. M. & WORSTER, M. G. 1995 Weakly nonlinear analysis of convection in mushy layers during the solidification of binary alloys. *J. Fluid Mech.* **302**, 307–331.
- ANDERSON, D. M. & WORSTER, M. G. 1996 A new oscillatory instability in a mushy layer during the solidification of binary alloys. *J. Fluid Mech.* **307**, 245–267.
- CHEN, F., LU, J. W. & YANG, T. L. 1994 Convective instability in ammonium chloride solution directionally solidified from below. *J. Fluid Mech.* **276**, 163–187.
- CHUNG, C. A. & CHEN, F. 2000 Onset of plume convection in mushy layers. *J. Fluid Mech.* **408**, 53–82.
- CRAWFORD, J. D. & KNOBLOCH, E. 1991 Symmetry and symmetry-breaking bifurcations in fluid dynamics. *Annu. Rev. Fluid Mech.* **23**, 341–387.
- DEANE, A. E., KNOBLOCH, E. & TOOMRE, J. 1987 Traveling waves and chaos in thermosolutal convection. *Phys. Rev. A* **36**, 2862–2869.
- EMMS, P. W. & FOWLER, A. C. 1994 Compositional convection in the solidification of binary alloys. *J. Fluid Mech.* **262**, 111–139.
- FEARN, D. R. 1998 Hydromagnetic flow in planetary cores. *Rep. Prog. Phys.* **61**, 175–235.
- FLEMINGS, M. C. 1974 *Solidification Processing*. McGraw Hill.
- FOWLER, A. C. 1985 The formation of freckles in binary alloys. *IMA J. Appl. Maths* **35**, 159–174.
- KERR, R. C. & TAIT, S. 1986 Crystallization and compositional convection in a porous medium with application to layered igneous intrusions. *J. Geophys. Res.* **91**, 3591–3608.
- KNOBLOCH, E. 1986 Oscillatory convection in binary mixtures. *Phys. Rev. A* **34**, 1538–1549.
- KNOBLOCH, E. & SILBER, M. 1990 Travelling wave convection in a rotating layer. *Geophys. Astrophys. Fluid Dyn.* **51**, 195–209.
- MALKUS, W. V. R. & VERONIS, G. 1958 Finite amplitude cellular convection. *J. Fluid Mech.* **4**, 225–260.
- MATTHEWS, P. C. & RUCKLIDGE, A. M. 1993 Travelling and standing waves in magnetoconvection. *Proc. R. Soc. Lond. A* **441**, 649–658.
- PALM, E., WEBER, J. E. & KVERNOLD, O. 1972 On steady convection in a porous medium. *J. Fluid Mech.* **54**, 153–161.
- RIahi, D. N. 2002 On nonlinear convection in mushy layers. Part 1. Oscillatory modes of convection. *J. Fluid Mech.* **467**, 331–359.
- SCHLUTER, A., LORTZ, D. & BUSSE, F. H. 1965 On the stability of steady finite amplitude convection. *J. Fluid Mech.* **23**, 129–144.
- SCHÖPF, W. & ZIMMERMANN, W. 1990 Results on wave patterns in binary fluid convection. *Phys. Rev. A* **41**, 1145–1148.
- SCHULZE, T. P. & WORSTER, M. G. 1999 Weak convection, liquid inclusions and the formation of chimneys in mushy layers. *J. Fluid Mech.* **388**, 197–215.
- SOLOMON, T. H. & HARTLEY, R. R. 1998 Measurements of the temperature field of mushy and liquid regions during solidification of aqueous ammonium chloride. *J. Fluid Mech.* **358**, 87–106.
- VERONIS, G. 1959 Cellular convection with finite amplitude in a rotating fluid. *J. Fluid Mech.* **5**, 401–435.
- WETTLAUER, J. S., WORSTER, M. G. & HUPPERT, H. E. 2000 Solidification of leads: theory, experiment and field observations. *J. Geophys. Res.* **105**, 1123–1135.
- WORSTER, M. G. 1992 Instabilities of the liquid and mushy regions during solidification of alloys. *J. Fluid Mech.* **237**, 649–669.
- WORSTER, M. G. 1997 Convection in mushy layers. *Annu. Rev. Fluid Mech.* **29**, 91–122.